Analytic properties of photonic crystal superprism parameters

M. J. Steel,[1,2] R. Zoli,[2,3] C. Grillet,[2] R. C. McPhedran,[2] C. Martijn de Sterke,[2] A. Norton,[4] P. Bassi,[3] and B. J. Eggleton[2]
[1]*RSoft Design Group, Inc., 65 O'Connor St, Chippendale, New South Wales 2008, Australia*
[2]*Centre for Ultrahigh-Bandwidth Devices for Optical Systems (CUDOS) and School of Physics, A28, University of Sydney, New South Wales 2006, Australia*
[3]*DEIS—Dipartimento di Elettronica Informatica e Sistemistica, University of Bologna, Viale Risorgimento 2, 40136 Bologna, Italy*
[4]*Centre for Ultrahigh-Bandwidth Devices for Optical Systems (CUDOS) and Department of Applied Mathematics, University of Technology, Sydney, New South Wales 2008, Australia*
(Received 6 October 2004; published 19 May 2005)

We study the analytic properties of the photonic crystal superprism resolution parameters *p*, *q*, and *r* introduced previously by Baba and Matsumoto [Appl. Phys. Lett. **81**, 2325 (2002)], which characterize the potential dispersive power of a superprism. We find closed form expressions for these quantities that greatly simplify their accurate evaluation and reveal significant insights about their behavior. The expressions imply general properties of the parameters which are true for all bands and all photonic crystals. In particular, we demonstrate that all photonic crystals exhibit infinite resolution as measured by the parameter *r* along particular contours in any photonic band.

DOI: 10.1103/PhysRevE.71.056608 PACS number(s): 42.25.Fx, 42.70.Qs, 42.82.Gw

I. INTRODUCTION

Photonic crystals, while still best known for their unique diffractive properties such as Bragg reflection, photonic band gaps, and strongly modified density of states, are increasingly attracting attention for their intriguing dispersive behavior within the photonic bands. Since being highlighted by Notomi [1], these dispersive properties have been explored in theory and experiment in the form of negative refraction [2–5], and more generally in the form of the *superprism* [6–11]. A superprism is a two-dimensional photonic crystal device, usually planar, that exhibits very strong angular steering of an output beam in response to modest changes in the angle or wavelength of an input beam. Such a device has obvious utility in applications such as switching, but also as an output coupler onto detector arrays [12].

The basic behavior of a superprism is commonly understood in terms of a momentum conservation argument based on the equifrequency contours of the two-dimensional in-plane band structure of the photonic crystal [1]. The standard construction is illustrated in Fig. 1. At the frequency of interest, the dispersion curves are drawn for an external uniform medium (thick circle) and photonic crystal (thin curve). The component of the incident wave vector **k** that is tangential to the interface between the two media (chain line) is conserved to within a reciprocal lattice vector upon refraction and determines the possible wave vectors $\boldsymbol{\kappa}$ within the photonic crystal. The normal to the photonic dispersion curve at $\boldsymbol{\kappa}$ gives the direction of energy flow within the crystal. In Fig. 1, only one of the two solutions carries energy into the crystal, and the other is disregarded. If the photonic crystal and the incoming beam are both very broad so that the approximation of plane-wave inputs is reasonable, this construction correctly predicts the propagation within the crystal.

However, as pointed out in a series of papers by Baba and co-workers [13–15], in order to design superprisms that work effectively, it is necessary to account for a number of additional factors. In practice, the plane-wave approximation is an imperfect one and the finite size of both the optical beams and the crystal plays an important role [16]. Since the angular spectrum of a Gaussian beam has a finite width in the plane-wave basis, different angular components undergo different degrees of refraction upon entering the crystal. This leads to beam spreading and a departure from the simple predictions of the geometric treatment above. To ensure that the refracted beam remains well collimated and to determine the ability of a crystal of a given size to separate incoming beams of different angles or frequencies, we must quantify the resolution properties of the superprism.

To this end, Baba and co-workers [13,14] introduced three standard parameters *p*, *q*, and *r* that relate the normalized optical frequency $\tilde{\omega} \equiv \omega/(2\pi c) = a/\lambda$, the propagation angle

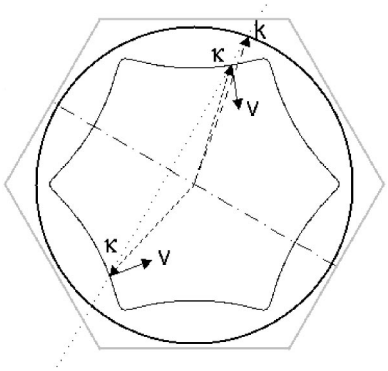

FIG. 1. Construction for refraction at the interface between a uniform medium and a photonic crystal. Equifrequency curves for a uniform (thick line) and triangular photonic crystal (fine line) are shown. Light is incident from a uniform medium with wave vector **k** upon an interface with the photonic crystal (chain line). The tangential wave vector component at the interface is conserved (dotted line) identifying the allowed output wave vectors $\boldsymbol{\kappa}$. The direction of the group velocity **v** in the photonic crystal is given by the normal to the equifrequency curve at its intersection with $\boldsymbol{\kappa}$.

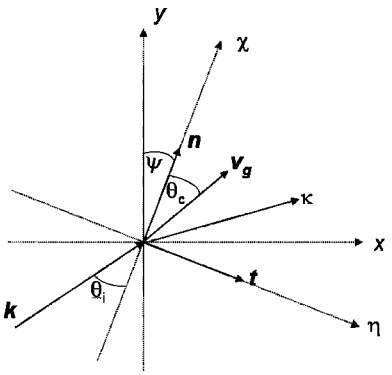

FIG. 2. Geometry for the superprism analysis. The coordinates (x,y) are the conventional coordinates of the Brillouin zone. The coordinates (η,χ) are aligned with the cut plane of the crystal which lies along the direction $\hat{\mathbf{t}}$. The angle $\psi=0$ if the crystal cut plane is along the Γ-X direction. The wave vector $\mathbf{k}$ represents the incoming beam at an angle θ_i to the normal to the interface $\hat{\mathbf{n}}$, and $\boldsymbol{\kappa}$ is the wave vector of the refracted beam inside the crystal. The angle between the normal $\hat{\mathbf{n}}$ and the group velocity $\mathbf{v}$ inside the crystal is denoted θ_c. The vectors $\boldsymbol{\kappa}$ and $\mathbf{v}$ are in general not collinear.

of the incoming beam θ_i and the propagation angle of the refracted beam θ_c. See Fig. 2 for the definitions of these angles, and note especially that θ_c is the angle of the group velocity inside the crystal, not of the wave vector $\boldsymbol{\kappa}$. The generalized angular resolving power, given by

$$p \equiv \left.\frac{\partial\theta_c}{\partial\theta_i}\right|_{\tilde{\omega}}, \tag{1}$$

measures the variation of output angle with input angle at fixed frequency. The generalized dispersion, given by

$$q \equiv \left.\frac{\partial\theta_c}{\partial\tilde{\omega}}\right|_{\theta_i}, \tag{2}$$

measures the change in the output angle with frequency at fixed input angle. Finally, the resolution parameter r satisfies

$$r \equiv \frac{q}{p} \equiv \left.\frac{\partial\theta_c}{\partial\tilde{\omega}}\right|_{\theta_i} \Bigg/ \left.\frac{\partial\theta_c}{\partial\theta_i}\right|_{\tilde{\omega}} = -\left.\frac{\partial\theta_i}{\partial\tilde{\omega}}\right|_{\theta_c}. \tag{3}$$

The resolution parameter scales the change of propagation angle with frequency, the most important attribute of a spectrometer, with the change of propagation angle with angle of incidence. The latter gives different frequency components the same propagation angle due to the range of angles present in the incident beam, and thus measures cross talk in the spectrometer. The three parameters p,q,r are defined throughout the first Brillouin zone, and every point in the zone corresponds to a particular experimental configuration of input angle θ_i and frequency $\tilde{\omega}$.

Using these three quantities, Baba and co-workers have explored a number of photonic crystal structures and superprism geometries in order to achieve high resolutions, and have identified structures with $r>75$. For comparison, conventional prisms have a resolution parameter of order unity.

However, several questions remain. Determination of the superprism parameters themselves is an intensive procedure since they depend on second derivatives of the photonic crystal dispersion relation, calculated along sharply curving contours. The difficulty of this is exacerbated by the high resolutions we have noted can occur in photonic crystals. For example, calculating p by first principles requires determining the group velocity $\mathbf{v}=\boldsymbol{\nabla}_{\mathbf{k}}\tilde{\omega}$ along an equifrequency contour, and implicitly parametrizing that contour with the input angle θ_i. Only then can the derivative $\partial\theta_c/\partial\theta_i|_{\tilde{\omega}}$, be evaluated. Since the equifrequency contours are strongly curved, this operation is numerically awkward, is ill suited to rectangular discretizations of the Brillouin zone, and is accurate only for extremely high-resolution sampling grids. Moreover, since the superprism parameters are found entirely numerically and are complicated functions, it is very difficult to develop much intuition for their general properties. Finally, the parameters have only been evaluated for the first few bands and for a limited range of photonic crystal designs. As such, it has not been possible to draw general conclusions regarding properties of arbitrary crystals or bands.

Here we provide answers to all these issues. Primarily, we find explicit analytic formulas for p, q, and r expressed only in terms of the incoming wave vector, and the standard first and second derivatives of the band surfaces with respect to the wave vector. This avoids the awkward process of calculating derivatives along curved arcs, and improves the accuracy of the results. In this way we show, for example, that the quantity p from Eq. (1) is closely related to the curvature of the equifrequency curves, as defined in the differential geometry of plane curves [17]. We also use these formulas to derive general properties about rotation of the crystal and the behavior of the parameters in any band of a photonic crystal. We show for instance that, for any photonic crystal, along a specific contour in the Brillouin zone, $p=0$. This contour then corresponds to a configuration in which the photonic crystal collimates the incident beam, with the result that the resolution parameter r diverges. That is, any band of any photonic crystal contains points of infinite resolution.

II. THEORY

We consider a two-dimensional photonic crystal, typically a square or triangular lattice with period a. As indicated in Fig. 2, light with wave vector $\mathbf{k}$ is incident from an external medium with refractive index n. In the external medium, we have the dispersion relation

$$\tilde{\omega} = \frac{a|\mathbf{k}|}{2\pi n}. \tag{4}$$

The refracted wave within the crystal must satisfy the dispersion relation of the crystal, that is, it must correspond to a solution $\tilde{\omega}=\tilde{\omega}_i(\boldsymbol{\kappa})$, for some photonic band i at a point $\boldsymbol{\kappa}$ within the first Brillouin zone.

We introduce two sets of coordinate axes in reciprocal space, (x,y) and (η,χ). The pair (x,y) are the natural coordinates of the Brillouin zone such that x lies along the Γ-X direction of the lattice. The coordinates (η,χ) are rotated by

an angle ψ so as to be aligned with the crystal interface. The two sets are thus related by

$$\begin{bmatrix} \eta \\ \chi \end{bmatrix} = \begin{bmatrix} \cos\psi & -\sin\psi \\ \sin\psi & \cos\psi \end{bmatrix} \begin{bmatrix} x \\ y \end{bmatrix}. \tag{5}$$

Note that the angle ψ depends only on the relative orientation of the interface between the uniform medium and the crystal, and the crystal lattice vectors. Thus $\psi=0$ when the interface tangent $\hat{\mathbf{t}}$ lies along the Γ-X direction.

Figure 2 is of course closely related to the construction in Fig. 1. The crystal interface indicated by the chain line in Fig. 1 corresponds to the η axis in Fig 2. Note that while there are two solutions for $\boldsymbol{\kappa}$ in Fig. 1, only one of them carries energy into the crystal and is of interest. The group velocities $\mathbf{v}$ in each figure correspond.

As mentioned previously, the internal and external wave vectors are related by the conservation of the tangential wave vector component at the interface, so that $(\mathbf{k}-\boldsymbol{\kappa})\cdot\hat{\mathbf{t}}=0$, or equivalently

$$k_\eta = \kappa_\eta, \tag{6}$$

where we use the notation $\mathbf{k}=(k_\eta,k_\chi)$ (see Fig. 1).

Now consider the directions of propagation of the incident and refracted beams. The group velocity in each medium is given by the gradient of the equifrequency curves,

$$\mathbf{v} = (v_\eta, v_\chi) = \boldsymbol{\nabla}_{\boldsymbol{\kappa}}\tilde{\omega}(\boldsymbol{\kappa}) = (\tilde{\omega}_{,\eta}, \tilde{\omega}_{,\chi}), \tag{7}$$

where subscripts after commas denote partial derivatives:

$$\tilde{\omega}_{,\eta} = \frac{\partial\tilde{\omega}}{\partial\eta}, \quad \tilde{\omega}_{,\chi} = \frac{\partial\tilde{\omega}}{\partial\chi}. \tag{8}$$

In the isotropic medium, $\mathbf{v}$ is parallel to the wave vector $\mathbf{k}$. In the photonic crystal, however, which behaves essentially as a dispersive anisotropic material, the group velocity and wave vector are in general not collinear. Thus, the incident and refracted angles, respectively, satisfy

$$\theta_i = \tan^{-1}\frac{k_\eta}{k_\chi}, \quad \theta_c = \tan^{-1}\frac{v_\eta}{v_\chi}. \tag{9}$$

A. Derivation of formulas

We now derive explicit formulas for the superprism parameters. In this section, we work exclusively in the (η,χ) coordinate system. Beginning with the resolving power p, elementary results give

$$p \equiv \left.\frac{\partial\theta_c}{\partial\theta_i}\right|_{\tilde{\omega}} \equiv \left.\frac{\partial}{\partial\theta_i}\right|_{\tilde{\omega}} \tan^{-1}(v_\eta/v_\chi)$$
$$= \frac{1}{|\mathbf{v}|^2}\left(v_\chi \left.\frac{\partial v_\eta}{\partial\theta_i}\right|_{\tilde{\omega}} - v_\eta \left.\frac{\partial v_\chi}{\partial\theta_i}\right|_{\tilde{\omega}}\right). \tag{10}$$

Since the equifrequency curves are complicated and can only be followed numerically, the derivatives of the group velocity components inside the parentheses of the final expression are awkward to calculate, and require a high sampling resolution for accuracy[13]. In Appendix A 1, we show how to write these expressions in terms of $\mathbf{k}$ and the standard partial derivatives $\tilde{\omega}_{,\eta}, \tilde{\omega}_{,\chi}$, and second derivatives $\tilde{\omega}_{,\eta\eta}, \tilde{\omega}_{,\eta\chi}, \tilde{\omega}_{,\chi\chi}$. The final expression for the angular resolving power is found to be

$$p = \frac{k_\chi}{\tilde{\omega}_{,\chi}}\left[\frac{1}{|\mathbf{v}|^2}(\tilde{\omega}_{,\eta\eta}\tilde{\omega}_{,\chi}{}^2 + \tilde{\omega}_{,\chi\chi}\tilde{\omega}_{,\eta}{}^2 - 2\tilde{\omega}_{,\eta\chi}\tilde{\omega}_{,\eta}\tilde{\omega}_{,\chi})\right]. \tag{11}$$

The dispersion parameter q is found in a similar fashion:

$$q \equiv \left.\frac{\partial\theta_c}{\partial\tilde{\omega}}\right|_{\theta_i} \equiv \left.\frac{\partial}{\partial\tilde{\omega}}\right|_{\theta_i} \tan^{-1}(v_\eta/v_\chi)$$
$$= \frac{1}{|\mathbf{v}|^2}\left(v_\chi \left.\frac{\partial v_\eta}{\partial\tilde{\omega}}\right|_{\theta_i} - v_\eta \left.\frac{v_\chi}{\partial\tilde{\omega}}\right|_{\theta_i}\right). \tag{12}$$

Using results in Appendix A 1, after some manipulation we find

$$q = \frac{k_\eta}{\tilde{\omega}_{,\chi}}\frac{1}{|\mathbf{v}|^2}\left[\frac{\tilde{\omega}_{,\eta\eta}\tilde{\omega}_{,\chi}{}^2 + \tilde{\omega}_{,\chi\chi}\tilde{\omega}_{,\eta}{}^2 - 2\tilde{\omega}_{,\eta\chi}\tilde{\omega}_{,\eta}\tilde{\omega}_{,\chi}}{\tilde{\omega}} + \frac{\tilde{\omega}_{,\chi}\tilde{\omega}_{,\eta\chi} - \tilde{\omega}_{,\eta}\tilde{\omega}_{,\chi\chi}}{k_\eta}\right] \tag{13}$$

$$= \frac{k_\eta}{k_\chi}\frac{p}{\tilde{\omega}} + \frac{1}{|\mathbf{v}|^2}\left(\frac{\tilde{\omega}_{,\chi}\tilde{\omega}_{,\eta\chi} - \tilde{\omega}_{,\eta}\tilde{\omega}_{,\chi\chi}}{\tilde{\omega}_{,\chi}}\right). \tag{14}$$

The resolution parameter is thus

$$r = \frac{1}{k_\chi}\left(\frac{k_\eta}{\tilde{\omega}} + \frac{\tilde{\omega}_{,\chi}\tilde{\omega}_{,\eta\chi} - \tilde{\omega}_{,\eta}\tilde{\omega}_{,\chi\chi}}{\tilde{\omega}_{,\eta\eta}\tilde{\omega}_{,\chi}{}^2 + \tilde{\omega}_{,\chi\chi}\tilde{\omega}_{,\eta}{}^2 - 2\tilde{\omega}_{,\eta\chi}\tilde{\omega}_{,\eta}\tilde{\omega}_{,\chi}}\right). \tag{15}$$

If desired, the final result may also be obtained by direct calculation of $\partial\theta_i/\partial\tilde{\omega}|_{\theta_c}$. Equations (11), (13), and (15) are the first principal results of the paper. Using these results, it is now elementary to construct detailed plots of these quantities throughout the Brillouin zone, without unduly high sampling resolution.

We indicated earlier that these expressions for p, p, and r improve the accuracy of their evaluation. It is true that both our formulas and the first principles definitions (1)–(3) require the calculation of numerical second derivatives, so at first sight both methods should be equally susceptible to numerical noise. However, note that in Eqs. (11), (13), and (15), the second derivatives appear explicitly and may be found by standard finite differences along the Cartesian axes η and χ, so that fourth order accuracy is easily obtained. In contrast, the second derivatives in Eqs. (1)–(3) are implicit. These formulas explictly involve only first derivatives, but they depend on the angle θ_c which is the direction of the gradient $\mathbf{v}$. As the derivatives are to be taken along complicated curves corresponding to fixed $\tilde{\omega}$, θ_i, or θ_c, it would be a nontrivial and tedious programming task to achieve fourth order accuracy using the first principles definitions.

B. The *p* parameter as a curvature

Equations (11)–(15) express the parameters in terms of the η,χ coordinate frame aligned with the external medium–

crystal interface. For both numerical convenience and physical insight it can be more helpful to express the quantities in terms of the Brillouin zone coordinates x,y. The various derivatives $\tilde{\omega}_{,\eta}$, $\tilde{\omega}_{,\chi}$, $\tilde{\omega}_{,\eta\eta}$, etc., are easily converted to the derivatives $\tilde{\omega}_{,x}$, $\tilde{\omega}_{,y}$, $\tilde{\omega}_{,xx}$, $\tilde{\omega}_{,xy}$, and $\tilde{\omega}_{,yy}$ using the transformation

$$\begin{bmatrix} \frac{\partial}{\partial \eta} \\ \frac{\partial}{\partial \chi} \end{bmatrix} = \begin{bmatrix} \cos\psi & -\sin\psi \\ \sin\psi & \cos\psi \end{bmatrix} \begin{bmatrix} \frac{\partial}{\partial x} \\ \frac{\partial}{\partial y} \end{bmatrix}. \tag{16}$$

Performing this transformation, we find in particular that the expression

$$G = \frac{\tilde{\omega}_{,\eta\eta}\tilde{\omega}_{,\chi}{}^2 + \tilde{\omega}_{,\chi\chi}\tilde{\omega}_{,\eta}{}^2 - 2\tilde{\omega}_{,\eta\chi}\tilde{\omega}_{,\eta}\tilde{\omega}_{,\chi}}{|\mathbf{v}|^3} \tag{17}$$

$$= \frac{\tilde{\omega}_{,xx}\tilde{\omega}_{,y}{}^2 + \tilde{\omega}_{,yy}\tilde{\omega}_{,x}{}^2 - 2\tilde{\omega}_{,xy}\tilde{\omega}_{,x}\tilde{\omega}_{,y}}{|\mathbf{v}|^3} \tag{18}$$

which appears in all three equations is invariant. In fact this is a well-known quantity—the *curvature* γ of the plane curve satisfying $\tilde{\omega}(x,y)=\tilde{\omega}_0$ [17], and defined as

$$\gamma = d\phi/ds, \tag{19}$$

where ϕ is the angle of the tangent vector $\mathbf{t}=(-\tilde{\omega}_{,y},\tilde{\omega}_{,x})$, and s is the arclength along the contour. Thus we have

$$p = \frac{k_\chi}{\tilde{\omega}_{,\chi}}|\mathbf{v}|G, \tag{20}$$

and using the relations $k_\chi=(2\pi n\tilde{\omega}/a)\cos\theta_i$ and $\tilde{\omega}_{,\chi}=|\mathbf{v}|\cos\theta_c$, we obtain the pleasing expression

$$p = \frac{\cos\theta_i}{\cos\theta_c}\frac{n2\pi\tilde{\omega}}{a}G. \tag{21}$$

Now it is straightforward to show that in a uniform isotropic medium of index n_i, $G=a/(2\pi n_i\tilde{\omega})$, and thus for an interface between two uniform media of indices n_1 and n_2,

$$p_{\text{uniform}} = \frac{n_1\cos\theta_i}{n_2\cos\theta_c}, \tag{22}$$

which can also be obtained directly from Eq. (1) in combination with Snell's law. Thus, finally, we have the result that for the photonic crystal, p can be considered as a factor due to a generalized Snell's law multiplied by the curvature of the equifrequency contour at the operating frequency. Below, we explore the physical significance of this result. Note finally that due to the invariance of G with respect to ψ, the only factor in Eq. (11) that gives p a dependence on the orientation of the crystal is the factor $k_\chi/\tilde{\omega}_\chi$. We discuss this further in Sec. III.

C. Alternate forms for *q*

Given the similarity of the definitions (1) and (2), it is natural to wonder whether q can be expressed in terms of the curvature of the contours of fixed input angle θ_i, just as p depends on the curvature of the equifrequency contours. However, the second term in Eq. (13) is not invariant under the coordinate transformation and such a relation does not exist. The reason of course, is that the output angle θ_c is still given by the normal to the equifrequency contours and so Eqs. (1) and (2) are not perfect analogs with respect to interchange of the variables. However, a little manipulation reveals the $q=(k_\chi/\tilde{\omega}_{,\chi})(\theta_{i,\eta}\theta_{c,\chi}-\theta_{i,\chi}\theta_{c,\eta})$. Thinking of the plane embedded in three space, this relation has a natural representation in terms of the vector cross product:

$$q = \frac{k_\chi}{\tilde{\omega}_{,\chi}}[(\boldsymbol{\nabla}_{\boldsymbol{\kappa}}(\theta_i),0)\times(\boldsymbol{\nabla}_{\boldsymbol{\kappa}}(\theta_c),0)]_z \tag{23}$$

$$= \frac{\cos\theta_i}{\cos\theta_c}\frac{n2\pi\tilde{\omega}}{a}\frac{1}{|\mathbf{v}|}[(\boldsymbol{\nabla}_{\boldsymbol{\kappa}}(\theta_i),0)\times(\boldsymbol{\nabla}_{\boldsymbol{\kappa}}(\theta_c),0)]_z \tag{24}$$

which contains the identical Snell's law factor seen in the second equality of Eq. (21).

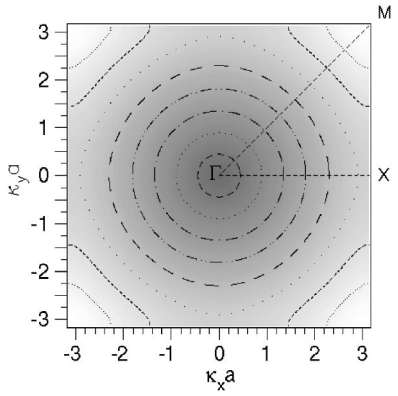

FIG. 3. Equifrequency contours and Brillouin zone for the first band of the photonic crystal with parameters given in the text. The band exhibits a (nondifferentiable) minimum at Γ, a saddle point at X, and a maximum at M.

III. FEATURES IN CONTOUR DIAGRAMS

From the work of Baba and co-workers [13,14], it is known that the superprism parameters p, q, and r show a surprising degree of fine structure. Using our expressions for these parameters, we can now understand the features in these diagrams. To begin, in Fig. 3 we show the equifrequency contours for the lowest band of a two-dimensional rectangular lattice of air holes in silicon (refractive index 3.065, period a, air hole radius $0.2635a$, corresponding to the configuration used in Ref. [15]). This band has a minimum at Γ at the Brillouin zone center, maxima at M, and saddle points at X. Figure 4 presents plots of the superprism parameters $\log_{10}|1/p|$, $\log_{10}|q|$, and $\log_{10}|r|$ for four different angles of incidence, 0°, 30°, 45°, and 70°. The incoming light is incident from a uniform medium with index 3.065. The quantities in these and all following plots were calculated with Eqs. (11)–(15) using the commercial band structure tool BandSOLVE [18].

In Fig. 4 we use the natural x,y coordinates in the Brillouin zone; the ξ,η system is rotated by ψ, with the short

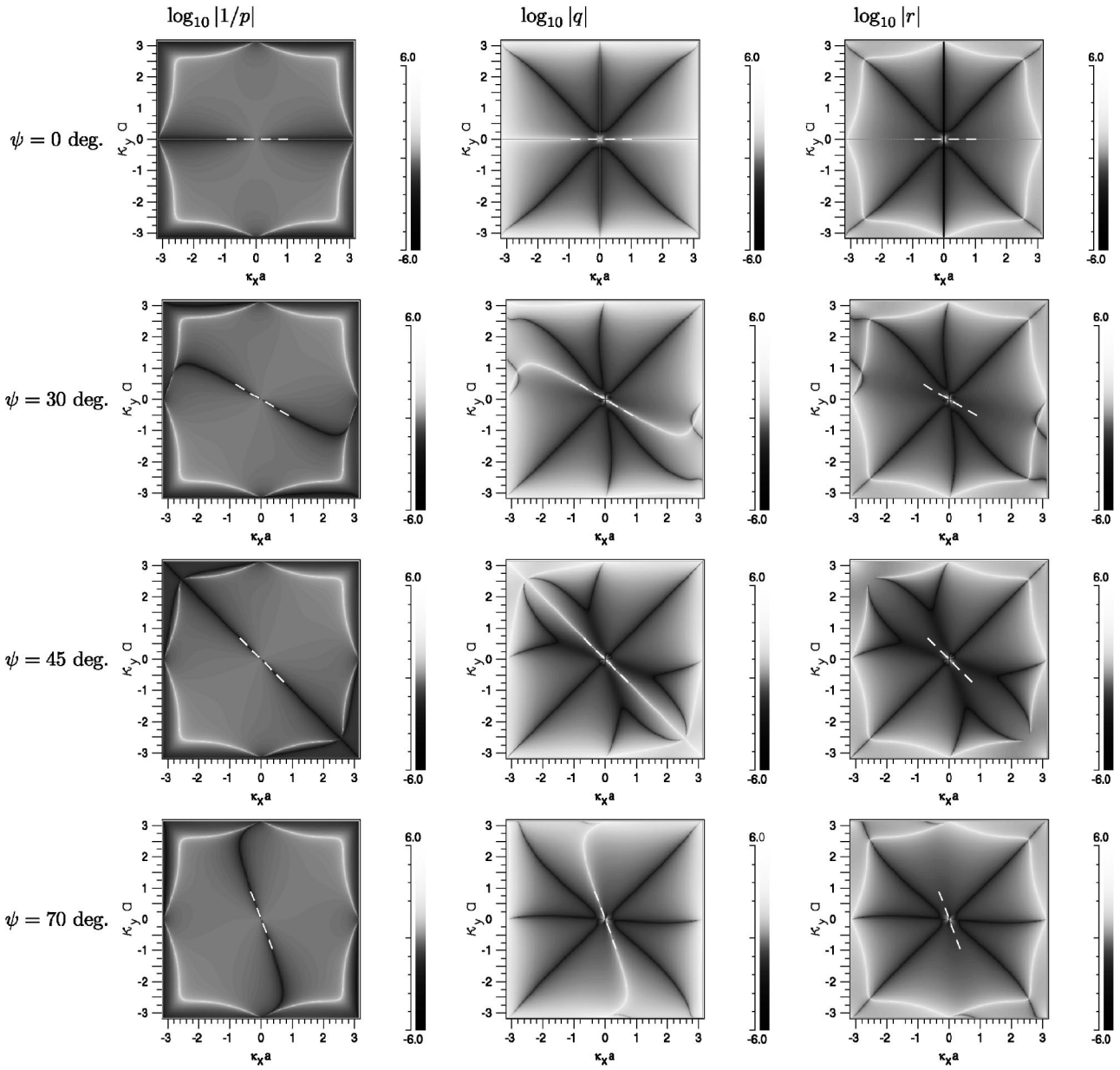

FIG. 4. Contour plots over the entire Brillouin zone of $\log_{10}|1/p|$, $\log_{10}|q|$, and $\log_{10}|r|$ (left to right) for a photonic crystal with parameters given in the text. The rows correspond to different orientations of the crystal cut plane with respect to the Γ-X direction. From the top, the angles are $\psi=0°$ (cut plane along Γ-X), 30°, 45° (cut plane along γ-M), and 70°. The broken white lines through the origin lie along the interface between the two media and thus indicate the direction of the η axis.

broken white lines through the origin denoting the direction of the η axis. Recall that a beam directed perpendicular to the η axis is normally incident upon the crystal.

A. Properties of p

Let us first consider the results for $|1/p|$ in the left column. We choose to plot $|1/p|$ rather than $|p|$ since then the logarithmic plots of $|r|$ can be understood as the sum of the corresponding plots of $|1/p|$ and $|q|$. In these plots, white indicates positive values, and black indicates negative regions. Thus since we are plotting $\log_{10}|1/p|$, white corresponds to small values of $|p|$ and black to large values of $|p|$.

Each $|1/p|$ plot shows two obvious features, a continuous white curve that passes through the X points (which we see below are saddle points of the band surface), and a black curve that passes through the origin. Note that the white curve is invariant with respect to ψ. In fact, it corresponds to the zeros of the curvature function G which depends only on the band structure and not on the interface properties. The physical relevance of the curvature is seen more clearly in Fig. 5 which superimposes $|1/p|$ with equifrequency contours for the first two bands. By definition [see Eq. (19)], the line of zero curvature $G=0$ traces out the inflection points of the equifrequency contours, as is apparent in Fig. 5. It is easy to understand why p should vanish at such points. Varying

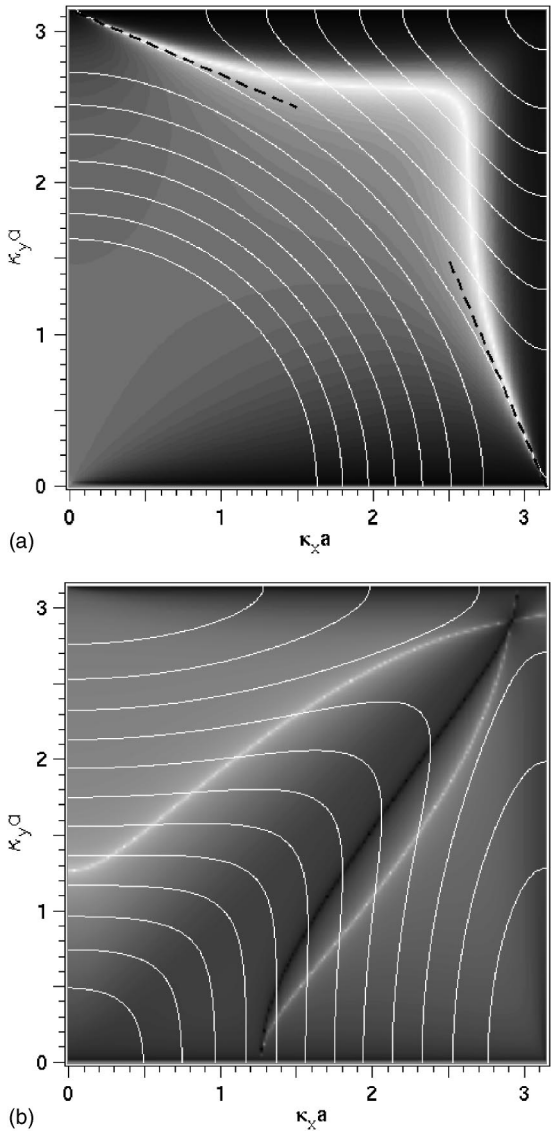

FIG. 5. Role of the curvature G in the structure of p for the lowest two bands at $\psi=0$. The peak of the diffuse white contour represents zeros of G. Thin white curves are the equifrequency contours of each band. For the lowest band, shown in (a) the black dotted lines indicate the direction of the $p=0$ curves obtained by quadratic expansion of the band at the saddle points at X. For the second band, shown in (b), there is a band maximum at Γ, minima at X and Y, and a saddle point just before M on Γ-M.

the input angle θ_i corresponds to moving along the equifrequency contour at the working frequency. Near an inflection point, the group velocity is constant to first order, and so the angle θ_c is also constant. By Eq. (1), we have $p=0$.

Note that in Fig. 5 for the second band we illustrate a case where the saddle point lies near but not exactly at M. The lines giving zeros of G intersect Γ-X and Γ-Y lines at right angles, and continue smoothly into the neighboring quadrants of the Brillouin zone.

Returning to the plots in the first column of Fig. 4, the black curve describes the locus of the function $\tilde{\omega}_{,\chi}=0$ or equivalently $\cos\theta_c=0$, which from Eq. (21) is the path along which p becomes singular. In theory, points near this curve exhibit very large angular resolving power. However, in practice, these regions are not very accessible, since with $\tilde{\omega}_{,\chi}\approx 0$, the group velocity is almost parallel to the interface of the crystal and the light travels almost parallel to the surface rather than through the crystal. It is interesting that at angles other than $\psi=0°$ and 45°, the curve $\tilde{\omega}_{,\chi}=0$ is not symmetric with respect to the normal to the interface. This is because at other values of ψ, the crystal does not have mirror symmetry in the direction of normal incidence and so the input angles $\pm\theta_i$ are not equivalent.

B. Properties of q

Consider now the plots of $|q|$ in the second column of Fig. 4. Again, the plots are characterized by fine lines of very large (white) and very small (black) values, but note that now both sets of curves depend on the interface angle ψ. The white maxima curves are identical to the minima in the $|1/p|$ plots. This is to be expected from the explicit dependence on p in Eq. (13). The complicated black minima curves obviously correspond to the cancellation of the two terms in Eq. (13), but more insight can be gained from Eq. (23). The cross product in that expression vanishes when the contours of input angle θ_i and output angle θ_c are locally tangent. This is illustrated in Fig. 6 which superimposes the contours of these angles with the $|q|$ function for three angles of ψ. The diffuse black contours corresponding to $q=0$ trace out the lines in the Brillouin zone where the two types of contours are locally parallel. This result has a simple physical interpretation. Recall that the q function is defined for constant input angle θ_i. Thus as the frequency is varied, we move along a contour of fixed θ_i. If this contour is tangent to a contour of fixed θ_c, then θ_c is unchanged as we sweep out the θ_i contour, and q vanishes. On the other hand, we would expect that the q function should be enhanced where the contours are locally perpendicular, but this effect tends to be swamped by the divergence of the $\cos\theta_c$ term in the denominator of Eq. (23).

C. Properties of r

The plots of $|r|$ in the third column of Fig. 4 are simply the sums of the previous two columns and there are no new features to explain. Typically, we are interested in regions of the Brillouin zone where r is large. However, noting that the largest values of r correspond to the zeros of G which are invariant with respect to the crystal orientation, we obtain the important result that rotating the crystal cannot improve the maximum potential values of r. However, rotations can make attractive parts of the Brillouin zone more *accessible*, by moving them away from points where $\tilde{\omega}_{,\chi}\approx 0$.

IV. GENERAL PROPERTIES OF THE PARAMETERS

The simple form (18) of the curvature G lets us make a number of general statements about the superprism parameters for all two-dimensional photonic crystals and all bands. In the figures already examined, paths of zero curvature were clearly visible. We now demonstrate that this is a universal property. We first recall the fundamental result that every photonic band contains several critical points within the Bril-

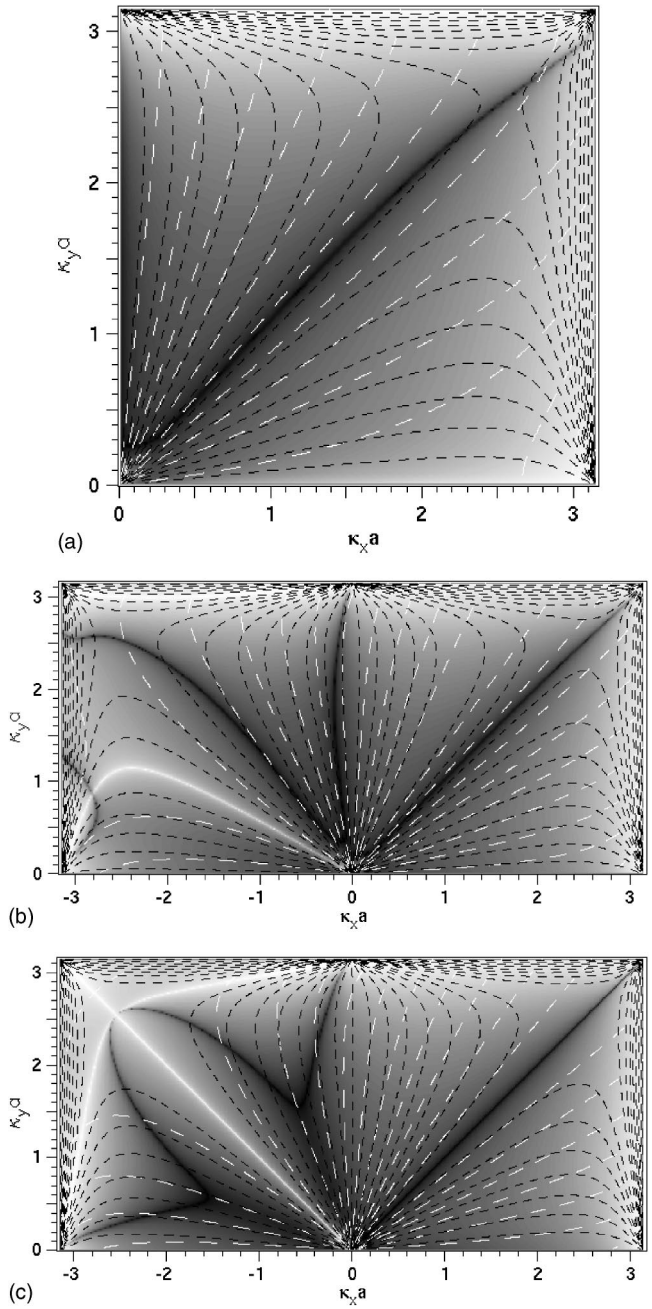

FIG. 6. Role of the isocontours of θ_i (dashed white) and θ_c (dashed black) in the structure of q for the lowest band at $\psi=0$ (left), 30° (center), and 45° (right). The diffuse black contour represents zeros of G.

louin zone. For two-dimensional photonic crystals, such as the structures we are considering here, the critical points include at least one minimum, one maximum, and two saddle points [19,20]. The group velocity vanishes at the critical points, so in the neighborhood of a critical point of frequency $\tilde{\omega}_0$, the frequency can be written as the quadratic form

$$\tilde{\omega} = \tilde{\omega}_0 + \frac{(\delta q_x)^2}{2C_x} + \frac{(\delta q_y)^2}{2C_y} \tag{25}$$

for constants C_x and C_y (these are similar to the effective masses in periodic electronic systems) [21]. At maxima or minima, C_x and C_y have the same sign, while they have opposite signs at saddle points. Now let $\delta q_y = \alpha \delta q_x$ for some α. Then near a critical point we have the quadratic expansion,

$$|\mathbf{v}|G = \frac{(1/C_x C_y)[1/C_x + \alpha^2/C_y]}{[1/C_x^2 + \alpha^2/C_y^2]}. \tag{26}$$

Thus as we approach a saddle point along the line $\alpha = \pm\sqrt{|C_x/C_y|}$, the quantity $|\mathbf{v}|G$ vanishes and since there are saddle points in every band, *there are positions where* $p=0$, *and therefore where* $r\to\infty$, *in every band for any photonic crystal*. This very general statement is the second principal result of this paper. Note that near these positions we expect a rapidly changing and very large but finite r. Of course, this argument does not apply to minima and maxima, for which C_x and C_y have the same sign.

In fact there are not just isolated points of vanishing G and thus infinite r, but continuous closed paths through the Brillouin zone. To see this, consider an irreducible segment of the Brillouin zone. Within this segment or on its boundary, there must exist a band maximum U_+ and minimum U_-. As is evident from the quadratic expansion (26), the quantity $|\mathbf{v}|G$ at U_+ and U_- has opposite signs. Then since $|\mathbf{v}|G$ is smooth, if we consider lines connecting U_+ and U_- and not leaving the segment, there must be an odd number of points along each line at which $|\mathbf{v}|G$ vanishes. By choosing arbitrary paths between U_+ and U_- we connect up such points of zero curvature to form trajectories. Since the curvature also vanishes at the saddle points in the segment, the saddle points must lie on the trajectories of zero curvature. If there is only one such trajectory it connects the two saddle points through the points of zero curvature on the lines from U_+ to U_-.

Before closing this section a few comments need to be made. The first is that in Eq. (25) we have taken the principal axes of the critical point to align with the coordinate axes. Though this is not true in general, the calculation is justified since the quantity $|\mathbf{v}|G$ is invariant under rotations. Second, note from Eq. (26) that $|\mathbf{v}|G$ is not uniquely defined at the critical points, varying between $1/C_x$ and $1/C_y$. However, this is only true at the critical points where $\mathbf{v}$ vanishes. Nonetheless, it shows that operating close to critical points is not desirable, unless $C_x = C_y$.

V. INFINITE *r* AND REAL SYSTEMS

Although we have drawn attention to the possibilities of zero diffraction along the lines where $p=0$, a real system can of course never attain this value, since the nonzero linewidths of the frequency and wave vector spectrum will smear out the values of the superprism parameters. Recall that through Eqs. (4) and (6), each incoming plane wave at a given frequency is mapped to a particular point in the Brillouin zone. Thus a distribution of incoming wave vectors and frequencies is mapped to a patch of the Brillouin zone. For a Gaussian beam of given angular spread Δk and linewidth $\Delta\omega$ say, it would be straightforward to determine the size of this patch and so obtain averaged values of p, q, and r. For cer-

tain problems, the minimum value over the patch might be more relevant than the average. A detailed analysis of the degree of averaging as a function of the beamwidth and linewidth is beyond the scope of this paper; however, one can imagine several ways to mitigate the problem. Of course, we can always reduce the impact of angular spreading by using a sufficiently large crystal and broad beam. However, certain portions of the Brillouin zone are intrinsically less sensitive to linewidth issues. For example, consider the "corner" of the $p=0$ curve in Fig. 5 at $(\kappa_x a, \kappa_y a) \approx (2.7, 2.7)$. The curvature of the equifrequency contour passing through this point vanishes to fourth order in $\delta\kappa$, and thus we would expect an optimal insensitivity to the angular spread of the incoming beam.

VI. CONCLUSION

We have provided convenient formulas for the calculation of the superprism parameters. Not only do these formulas simplify the analysis of superprism performance, but they also show that infinite resolution as determined by the parameter r is theoretically attainable in any crystal and any band. The art of superprism design is to obtain strong resolution, yet over reasonable bandwidths, and to combine this with good energy efficiency. The accurate and computationally efficient formulas derived here and the identification of the region in the Brillouin zone associated with very high resolution should help future research aimed at exploring applications and devices based on superprism phenomena in photonic crystals.

ACKNOWLEDGMENTS

This work was supported by the Australian Research Council under the ARC Centres of Excellence program and by a grant from the Defence Science and Technology Organization. R.Z. was supported by a Marco Polo Research and International Relations Grant.

APPENDIX A: EVALUATION OF DERIVATIVES ALONG EQUIFREQUENCY CONTOURS

1. Derivatives needed for *p*

By simple geometry, we can consider the incoming wave vector $\mathbf{k}$ as a function of θ_i and $\tilde{\omega}$,

$$\mathbf{k}(\theta_i, \tilde{\omega}) = \frac{2\pi n \tilde{\omega}}{a}(\sin\theta_i, \cos\theta_i). \tag{A1}$$

Figure 1 indicates how to find $\boldsymbol{\kappa}$ given $\mathbf{k}$ so it is reasonable to view the in-crystal wave vector as a function $\boldsymbol{\kappa}(\mathbf{k})$ of the incoming wave vector. Thus the group velocity $\mathbf{v}(\boldsymbol{\kappa})$ has the complete dependence $\mathbf{v}\{\boldsymbol{\kappa}[\mathbf{k}(\theta_i, \tilde{\omega})]\}$ By the chain rule, we can write

$$\left.\frac{\partial v_j}{\partial \theta_i}\right|_{\tilde{\omega}} = \frac{\partial v_j}{\partial \kappa_l}\left.\frac{\partial \kappa_l}{\partial \theta_i}\right|_{\tilde{\omega}} = \frac{\partial v_j}{\partial \kappa_l}\frac{\partial \kappa_l}{\partial k_m}\left.\frac{\partial k_m}{\partial \theta_i}\right|_{\tilde{\omega}} \tag{A2}$$

$$= \frac{\partial^2 \tilde{\omega}}{\partial \kappa_j \partial \kappa_l}\frac{\partial \kappa_l}{\partial k_m}\left.\frac{\partial k_m}{\partial \theta_i}\right|_{\tilde{\omega}}. \tag{A3}$$

Here repeated indices indicate a sum over the coordinates χ and η and we used $v_j = \partial\tilde{\omega}/\partial\kappa_j$. The first term in Eq. (A3) is the standard second derivative $\tilde{\omega}_{,jl}$. We now need to simplify the other derivatives $\partial\kappa_l/\partial k_m$ and $(\partial k_m/\partial\theta_i)|_{\tilde{\omega}}$. For the first of these, we find the inverse of the matrix of reciprocal derivatives:

$$\frac{\partial \kappa_j}{\partial k_l} = \left[\frac{\partial k_j}{\partial \kappa_l}\right]^{-1} = \begin{bmatrix} \frac{\partial k_\eta}{\partial \kappa_\eta} & \frac{\partial k_\eta}{\partial \kappa_\chi} \\ \frac{\partial k_\chi}{\partial \kappa_\eta} & \frac{\partial k_\chi}{\partial \kappa_\chi} \end{bmatrix}^{-1} \tag{A4}$$

$$= \begin{bmatrix} 1 & 0 \\ \left(\frac{2\pi n}{a}\right)^2 \frac{\tilde{\omega}\tilde{\omega}_{,\eta}}{k_\chi} - \frac{k_\eta}{k_\chi} & \left(\frac{2\pi n}{a}\right)^2 \frac{\tilde{\omega}\tilde{\omega}_{,\chi}}{k_\chi} \end{bmatrix}^{-1}$$

$$= \begin{bmatrix} 1 & 0 \\ \frac{\tilde{\omega}_{,\eta}}{k_\chi (2\pi n/a)^2 \tilde{\omega}} - \frac{\tilde{\omega}_{,\eta}}{\tilde{\omega}_{,\chi}} & \frac{k_\chi}{(2\pi n/a)^2 \tilde{\omega}\tilde{\omega}_{,\chi}} \end{bmatrix}. \tag{A5}$$

Here we have used Eqs. (4) and (6), in progressing from the first to the second line.

Finally, to obtain $\partial k_j/\partial\theta_i$, we introduce a new coordinate pair $\delta = (\theta_i, \tilde{\omega})$, so that $\partial k_j/\partial\theta_i = \partial k_j/\partial\delta_1$. Then, proceeding as before we have

$$\frac{\partial k_j}{\partial \delta_l} = \left[\frac{\partial \delta_j}{\partial k_l}\right]^{-1} = \begin{bmatrix} \frac{\partial \theta_i}{\partial k_\eta} & \frac{\partial \theta_i}{\partial k_\chi} \\ \frac{\partial \tilde{\omega}}{\partial k_\eta} & \frac{\partial \tilde{\omega}}{\partial k_\chi} \end{bmatrix}^{-1} \tag{A6}$$

$$= \left(\frac{1}{(2\pi a/n)^2 \tilde{\omega}} \begin{bmatrix} \frac{k_\chi}{\tilde{\omega}} & \frac{-k_\eta}{\tilde{\omega}} \\ k_\eta & k_\chi \end{bmatrix}\right)^{-1} = \begin{bmatrix} k_\chi & \frac{k_\eta}{\tilde{\omega}} \\ -k_\eta & \frac{k_\chi}{\tilde{\omega}} \end{bmatrix}. \tag{A7}$$

Combining Eqs. (A5) and (A7) with the last of Eq. (10) yields Eq. (11).

2. Derivatives needed for *q*

The procedure for the derivatives required for q is similar. This time, we have

$$\left.\frac{\partial v_j}{\partial \tilde{\omega}}\right|_{\theta_i} = \frac{\partial v_j}{\partial \kappa_l}\left.\frac{\partial \kappa_l}{\partial \tilde{\omega}}\right|_{\theta_i} \tag{A8}$$

$$= \frac{\partial v_j}{\partial \kappa_l}\frac{\partial \kappa_l}{\partial k_m}\left.\frac{\partial k_m}{\partial \tilde{\omega}}\right|_{\theta_i} \tag{A9}$$

$$= \frac{\partial^2 \tilde{\omega}}{\partial \kappa_j \partial \kappa_l}\frac{\partial \kappa_l}{\partial k_m}\left.\frac{\partial k_m}{\partial \tilde{\omega}}\right|_{\theta_i}. \tag{A10}$$

Since $\partial k_m/\partial\tilde{\omega}|_{\theta_i} = \partial k_m/\partial\delta_2$, Eqs. (A5) and (A7) provide the remaining unknowns in Eq. (A10), which substituted into the last of Eq. (12) gives Eq. (13).

[1] M. Notomi, Phys. Rev. B **62**, 10696 (2000).
[2] J. B. Pendry, Contemp. Phys. **45**, 191 (2004).
[3] P. V. Parimi, W. T. Lu, P. Vodo, J. Sokoloff, J. S. Derov, and S. Sridhar, Phys. Rev. Lett. **92**, 127401 (2004).
[4] A. Berrier, M. Mulot, M. Swillo, M. Qiu, L. Thylen, A. Talneau, and S. Anand, Phys. Rev. Lett. **93**, 073902 (2004).
[5] B. Gralak *et al.*, J. Opt. Soc. Am. A **17**, 1012 (2000).
[6] H. Kosaka, T. Kawashima, A. Tomita, M. Notomi, T. Tamamura, T. Sato, and S. Kawakami, Phys. Rev. B **58**, R10096 (1998).
[7] H. Kosaka, T. Kawashima, A. Tomita, M. Notomi, T. Tamamura, T. Sato, and S. Kawakami, Appl. Phys. Lett. **7**, 1370 (1999).
[8] H. Kosaka, T. Kawashima, A. Tomita, M. Notomi, T. Tamamura, T. Sato, and S. Kawakami, J. Lightwave Technol. **17**, 2032 (1999).
[9] L. Wu, M. Mazilu, T. Karle, and T. F. Krauss, IEEE J. Quantum Electron. **38**, 915 (2002).
[10] D. N. Chigrin, S. Enoch, C. M. S. Torres, and G. Tayeb, Opt. Express **11**, 1203 (2003).
[11] A. L. Cabuz *et al.*, Appl. Phys. Lett. **84**, 2031 (2004).
[12] B. Momeni *et al.*, Appl. Phys. B: Lasers Opt. **77**, 555 (2003).
[13] T. Baba and M. Nakamura, IEEE J. Quantum Electron. **38**, 909 (2002).
[14] T. Baba and T. Matsumoto, Appl. Phys. Lett. **81**, 2325 (2002).
[15] T. Matsumoto and T. Baba, J. Lightwave Technol. **22**, 917 (2004).
[16] D. Felbacq and R. Smaâli, Phys. Rev. Lett. **92**, 193902 (2004).
[17] M. P. do Carmo, *Differential Geometry of Curves and Surfaces* (Prentice-Hall, Englewood Cliffs, NJ, 1976), Chap. 1.
[18] Available at www.rsoftdesign.com
[19] R. C. McPhedran, L. C. Botten, J. McOrist, A. A. Asatryan, C. M. de Sterke, and N. A. Nicorovici, Phys. Rev. E **69**, 016609 (2004).
[20] F. Bassani and G. P. Parravicini, *Electronic States and Optical Transitions in Solids* (Pergamon Press, New York, 1975).
[21] Note that the minimum of the lowest band at Γ is not quadratic as in Eq. (25), but rather cone shaped, as for an isotropic medium. However, this very isotropy makes the minimum uninteresting in terms of designing superprisms, so this is not a significant problem.